



## Synthesis of novel diketopyrrolopyrrole-based luminophores showing crystallization-induced emission enhancement properties

Yi Jin<sup>a</sup>, Yanbin Xu<sup>a</sup>, Yinling Liu<sup>a</sup>, Lingyun Wang<sup>a</sup>, Huanfeng Jiang<sup>a</sup>, Xianjie Li<sup>b</sup>, Derong Cao<sup>a,\*</sup>

<sup>a</sup>School of Chemistry and Chemical Engineering, South China University of Technology, 381 Wushan Road, Guangzhou 510641, China

<sup>b</sup>State Key Laboratory of Supramolecular Structure and Materials, Jilin University, Changchun 130012, China

### ARTICLE INFO

#### Article history:

Received 16 September 2010

Received in revised form

10 January 2011

Accepted 11 January 2011

Available online 19 January 2011

#### Keywords:

Diketopyrrolopyrrole

Crystallization-induced emission enhancement

Fluorescence

Restriction of intramolecular rotation

Aggregate-induced emission

### ABSTRACT

A series of diketopyrrolopyrrole-based luminophores were synthesized and characterized. Their photoluminescent properties were affected significantly by the change of  $\pi$ -conjugated units and alkyl groups linked to the diketopyrrolopyrrole-ring. 2,5-Dialkyl-3,6-bis(4-((10-oxoanthracen-9(10H)-ylidene)methyl)phenyl)pyrrolo[3,4-c]pyrrole-1,4-dione showed aggregate-induced emission enhancement and crystallization-induced emission enhancement properties while 3,6-bis(4-[1,3]dioxolan-2-yl-phenyl)-2,5-dialkylpyrrolo[3,4-c]pyrrole-1,4-dione, 2,5-dialkyl-3,6-bis(4-formylphenyl)pyrrolo[3,4-c]pyrrole-1,4-dione, and 2,5-dioctyl-3,6-bis(4-[2-(4-bromophenyl)-2-cyanovinyl]-phenyl)pyrrolo[3,4-c]pyrrole-1,4-dione did not exhibit these properties. The results showed that emission enhancements of the luminophores depended on the competition between the restriction of intramolecular rotation and  $\pi$ - $\pi$  aggregation with the former causing emission enhancement and the latter inducing fluorescence quenching.

© 2011 Elsevier Ltd. All rights reserved.

### 1. Introduction

$\pi$ -Conjugated organic materials have recently attracted much attention because of their potential applications in biological imaging systems [1,2] and light-emitting diodes [3,4]. It is necessary to understand and to manipulate their solid-state optical properties for achieving successful functional devices containing  $\pi$ -conjugated materials.

In the solid state, luminogenic molecules lie in close proximity and form aggregates. Chromophore aggregation usually quenches the emission of organic luminophores which have high luminescence efficiencies in dilute solutions. Such quenching is due to the formation of detrimental species such as excimers [5–8]. However, a novel phenomenon, aggregate-induced emission enhancement (AIEE) or aggregate-induced emission (AIE), has been recently reported [9]. This emission phenomenon is manifest by compounds exhibiting significant enhancement of their light-emission in the amorphous or crystalline states whereas they exhibit weak or almost no emission in dilute solutions. Furthermore, the crystals of some compounds emit more efficiently than their solution or amorphous powders, showing a novel phenomenon of crystallization-induced

emission or crystallization-induced emission enhancement (CIEE) [9,10]. High-tech applications of the AIE luminogens are explored, for example, in fluorescence sensors, biological probes, immunoassay markers, poly(acrylamide) gel electrophoresis visualization agents, monitors for layer-by-layer assembly, reporters for micelle formation and multi-stimuli-responsive nanomaterials [9]. However, only a limited number of organic compounds display AIE characteristics such as siloles, aminobenzoic acids, arylethene and arylbenzene derivatives [7,9–17].

Some hypotheses have been proposed for the possible mechanism of AIE. Generally, AIE has been attributed to the restriction of intramolecular rotations (RIR) [9,18–21], formation of J-aggregates [22,23], intramolecular planarization [5] or restriction of the transition from the local excited state to the intramolecular charge transfer state that accompanies twisting [24].

The nature of molecular aggregation in bulk is controlled by a delicate balance of various weak intermolecular forces including both  $\pi$ -conjugated units and remote functional groups which are not in conjugation [25,26]. Therefore, variations in the structure of  $\pi$ -conjugated units and the remote functional groups could be utilized as an effective strategy to fine-tune the solid-state photophysical properties of a luminophore [27]. Diketopyrrolopyrrole (DPP) derivatives are a class of strongly fluorescent heterocyclic pigments and their structures can be easily optimized through variations of substituents at the 2,5- and 3,6-positions [28,29].

\* Corresponding author. Tel./fax: +86 20 87110245.

E-mail address: [drcao@scut.edu.cn](mailto:drcao@scut.edu.cn) (D. Cao).

In this study, in order to enlarge the family of AIE luminophores and to gain an insight into luminogenic molecular structure–property relationships, a series of new DPP derivatives with systematically varied substituents at the 2,5- and 3,6-positions were synthesized. We also studied the influence of  $\pi$ -conjugated units and alkyl substituents linked to the DPP-ring upon emission behavior of the DPP-luminophores in both solution and solid state.

## 2. Experimental section

### 2.1. Instrumentation and materials

NMR ( $^1\text{H}$  and  $^{13}\text{C}$ ) spectra were collected on a Bruker DRX 400 spectrometer (in  $\text{CDCl}_3$  or  $\text{DMSO}-d_6$ , TMS as internal standard). MALDI-TOF mass spectra were recorded on a Bruker Autoflex TOF mass spectrometer. APCI-MS spectra were recorded with a Bruker Esquire HCT plus mass spectrometer. Elemental analyses were performed using a Vario EL III instrument. Fourier transform infrared (FT-IR) spectra were recorded on an RFX-65A (Analect Co.) spectrometer. UV–vis absorption spectra were obtained on a Shimadzu UV-2550 spectrometer. PL spectra were obtained on a Hitachi F-4500 FL Spectrophotometer. PL quantum yields in solution were estimated using Rhodamine 6G ( $\phi_F = 95\%$  in ethanol) as the standard,  $\lambda_{\text{ex}} = 488 \text{ nm}$  [30,31]. The absolute PL quantum yields were determined in an Integrating sphere IS080 (Labsphere) with 325 nm excitation of He–Cd laser (Mells Grid), as a percent of the total output photons in all directions vs the total input photons. Single crystal X-ray diffraction intensity data were collected on a Bruker Smart 1000 CCD diffractometer. Polarizing optical micrographs were observed with a polarized light microscope Olympus BX41.

Ethanol was distilled from sodium under nitrogen. *N*-Methyl-2-pyrrolidone (NMP) was dried with  $\text{CaH}_2$  and distilled under nitrogen atmosphere. Other solvents were obtained from commercially available resources without further purification. Compounds **1**, **2a**, **3a** were synthesized according to the published literature [32].

### 2.2. Syntheses of DPP derivatives 2–5

#### 2.2.1. 3,6-Bis(4-[1,3]dioxolan-2-yl-phenyl)-2,5-dibutylpyrrolo[3,4-c]pyrrole-1,4-dione (**2b**)

A mixture of 3,6-bis(4-[1,3]dioxolan-2-yl-phenyl)pyrrolo[3,4-c]pyrrole-1,4-dione (**1**) (2.00 g, 4.63 mmol), potassium *tert*-butoxide (2.59 g, 23.1 mmol), and dry NMP (60 mL) was heated to 60 °C and stirred for 0.5 h. 1-Bromobutane (3.8 g, 27.8 mmol) in dry NMP (30 mL) was added dropwise to the mixture which was stirred at 60 °C for 10 h under nitrogen atmosphere. The solvent was evaporated under reduced pressure and the residue was purified by silica gel column (eluent: petroleum ether/dichloromethane/ethyl acetate 5:5:1) to afford a yellow solid (**2b**) in 45% yield (1.13 g), m.p. 229–230 °C. FT-IR (KBr,  $\text{cm}^{-1}$ ): 3063, 2950, 2928, 2869, 1667, 1603, 1509, 1454, 1384, 1084, 727.  $^1\text{H}$  NMR (400 MHz,  $\text{CDCl}_3$ , ppm):  $\delta$  7.81 (d,  $J = 8.4 \text{ Hz}$ , 4H, Ar), 7.62 (d,  $J = 8.0 \text{ Hz}$ , 4H, Ar), 5.87 (s, 2H, OCHO), 4.13–4.05 (m, 8H,  $\text{OCH}_2\text{CH}_2\text{O}$ ), 3.74–3.70 (m, 4H,  $\text{NCH}_2$ ), 1.58–1.50 (m, 4H,  $\text{CH}_2$ ), 1.26–1.20 (m, 4H,  $\text{CH}_2$ ), 0.82 (t,  $J = 7.2 \text{ Hz}$ , 6H,  $\text{CH}_3$ );  $^{13}\text{C}$  NMR (100 MHz,  $\text{CDCl}_3$ , ppm)  $\delta$  162.5, 148.0, 140.9, 128.8, 128.7, 126.9, 109.9, 102.9, 65.3, 41.6, 31.5, 19.9, 13.5; MS (APCI) calcd for  $\text{C}_{32}\text{H}_{36}\text{N}_2\text{O}_6$  544.3, found 545.2. Anal. Calc. for  $\text{C}_{32}\text{H}_{36}\text{N}_2\text{O}_6$ : C, 70.57; H, 6.66; N, 5.14. Found: C, 70.40; H, 6.69; N, 5.14.

#### 2.2.2. 3,6-Bis(4-[1,3]dioxolan-2-yl-phenyl)-2,5-dibenzylpyrrolo[3,4-c]pyrrole-1,4-dione (**2c**)

A mixture of **1** (2.00 g, 4.63 mmol), potassium *tert*-butoxide (2.59 g, 23.1 mmol), and dry NMP (60 mL) was stirred for 0.5 h at 20 °C. Benzyl bromide (4.75 g, 27.8 mmol) in dry NMP (30 mL) was

added dropwise to the mixture which was stirred at 20 °C for 10 h under nitrogen. Then, the solvent was evaporated under reduced pressure and the residue was recrystallized with NMP and methanol to afford a yellow solid (**2c**) in 44% yield (1.25 g), m.p. 285–287 °C. FT-IR (KBr,  $\text{cm}^{-1}$ ): 3060, 2920, 2883, 1687, 1603, 1509, 1451, 1072, 840.  $^1\text{H}$  NMR (400 MHz,  $\text{CDCl}_3$ , ppm):  $\delta$  7.75 (d,  $J = 8.0 \text{ Hz}$ , 4H, Ar), 7.53 (d,  $J = 8.4 \text{ Hz}$ , 4H, Ar), 7.31–7.17 (m, 10H, Ar), 5.83 (s, 2H, OCHO), 4.95 (s, 4H,  $\text{NCH}_2$ ), 4.09–4.02 (m, 8H,  $\text{OCH}_2\text{CH}_2\text{O}$ );  $^{13}\text{C}$  NMR (100 MHz,  $\text{CDCl}_3$ , ppm)  $\delta$  162.7, 148.7, 141.3, 137.4, 129.1, 128.8, 128.4, 127.4, 126.9, 126.6, 109.8, 102.9, 65.3, 45.6; MS (APCI) calcd for  $\text{C}_{38}\text{H}_{32}\text{N}_2\text{O}_6$  612.2, found 613.1. Anal. Calc. for  $\text{C}_{38}\text{H}_{32}\text{N}_2\text{O}_6$ : C, 74.49; H, 5.26; N, 4.57. Found: C, 74.31; H, 5.34; N, 4.56.

#### 2.2.3. 2,5-Dibutyl-3,6-bis(4'-formylphenyl)pyrrolo[3,4-c]pyrrole-1,4-dione (**3b**)

A mixture of **2b** (0.916 g, 1.68 mmol), THF (100 mL) and HCl (2.0 mol/L, 8.5 mL) was stirred at 60 °C for 2 h. The solvent was removed and the residue was washed with water to afford an orange solid (**3b**) in 99% yield (0.737 g), m.p. 184–186 °C. FT-IR (KBr,  $\text{cm}^{-1}$ ): 2957, 2930, 2869, 2751, 1702, 1667, 1592, 1505, 1457, 1392, 1089, 830, 738.  $^1\text{H}$  NMR (400 MHz,  $\text{CDCl}_3$ , ppm)  $\delta$  10.06 (s, 2 H, CHO), 8.01–7.94 (m, 8H, Ar), 3.75 (t,  $J = 8.0 \text{ Hz}$ , 4H,  $\text{NCH}_2$ ), 1.52 (m, 4H,  $\text{CH}_2$ ), 1.25–1.20 (m, 4H,  $\text{CH}_2$ ), 0.81 (t,  $J = 8.0 \text{ Hz}$ , 6H,  $\text{CH}_3$ );  $^{13}\text{C}$  NMR (100 MHz,  $\text{CDCl}_3$ , ppm)  $\delta$  191.2, 162.2, 147.6, 137.6, 133.2, 129.9, 129.2, 111.0, 41.7, 31.5, 19.9, 13.5; MS (APCI) calcd for  $\text{C}_{28}\text{H}_{28}\text{N}_2\text{O}_4$  456.2, found 457.1. Anal. Calc. for  $\text{C}_{28}\text{H}_{28}\text{N}_2\text{O}_4$ : C, 73.66; H, 6.18; N, 6.14. Found: C, 73.58; H, 6.23; N, 6.14.

#### 2.2.4. 2,5-Dibenzyl-3,6-bis(4'-formylphenyl)pyrrolo[3,4-c]pyrrole-1,4-dione (**3c**)

It was prepared by using the same synthetic procedure of **3b** to afford an orange solid (**3c**) in 98% yield, m.p. 258–259 °C. FT-IR (KBr,  $\text{cm}^{-1}$ ): 2927, 2845, 2742, 1703, 1674, 1594, 1505, 1456, 833.  $^1\text{H}$  NMR (400 MHz,  $\text{DMSO}-d_6$ , ppm)  $\delta$  10.05 (s, 2H, CHO), 8.01 (d,  $J = 8.0 \text{ Hz}$ , 4H, Ar), 7.97 (d,  $J = 8.0 \text{ Hz}$ , 4H, Ar), 7.29–7.09 (m, 10H, Ar), 5.00 (s, 4H,  $\text{NCH}_2$ );  $^{13}\text{C}$  NMR (100 MHz,  $\text{DMSO}-d_6$ , ppm)  $\delta$  192.6, 161.5, 147.5, 137.5, 137.1, 132.4, 129.6, 129.4, 128.7, 127.3, 126.5, 110.2, 44.5; MS (APCI) calcd for  $\text{C}_{34}\text{H}_{24}\text{N}_2\text{O}_4$  524.2, found 525.1. Anal. Calc. for  $\text{C}_{34}\text{H}_{24}\text{N}_2\text{O}_4$ : C, 77.85; H, 4.61; N, 5.34. Found: C, 77.69; H, 4.65; N, 5.32.

#### 2.2.5. 2,5-Dioctyl-3,6-bis(4'-((10-oxoanthracen-9(10H)-ylidene)methyl)phenyl)pyrrolo[3,4-c]pyrrole-1,4-dione (**4a**)

Anthrone (404 mg, 2.08 mmol) and **3a** (473 mg, 0.832 mmol) were mixed in absolute ethanol (20 mL). Then the suspension was saturated with gaseous HCl overnight and then heated under reflux for 3.5 h. After cooling, the mixture was poured into  $\text{H}_2\text{O}$ . Precipitates were washed with methanol and recrystallized with  $\text{CH}_2\text{Cl}_2$  and methanol to afford a red solid (**4a**) in 74.1% yield (568 mg), m.p. 270–271 °C. FT-IR (KBr,  $\text{cm}^{-1}$ ): 3059, 3035, 2951, 2921, 2850, 1659, 1592, 1503, 1462, 1087, 780, 722.  $^1\text{H}$  NMR (400 MHz,  $\text{CDCl}_3$ , ppm)  $\delta$  8.32–8.27 (m, 4H, Ar), 8.05 (d,  $J = 8.0 \text{ Hz}$ , 2H, Ar), 7.82 (d,  $J = 8.0 \text{ Hz}$ , 4H, Ar), 7.69 (t,  $J = 8.0 \text{ Hz}$ , 2H, Ar), 7.60 (d,  $J = 8.0 \text{ Hz}$ , 2H, Ar), 7.56–7.47 (m, 10H, Ar and C=CH), 7.26 (t,  $J = 8.0 \text{ Hz}$ , 2H, Ar), 3.78 (t,  $J = 8.0 \text{ Hz}$ , 4H,  $\text{NCH}_2$ ), 1.63 (m, 4H,  $\text{CH}_2$ ), 1.25–1.21 (m, 20H,  $\text{CH}_2$ ), 0.84 (t,  $J = 8.0 \text{ Hz}$ , 6H,  $\text{CH}_3$ );  $^{13}\text{C}$  NMR (100 MHz,  $\text{CDCl}_3$ , ppm)  $\delta$  184.6, 162.6, 147.7, 140.3, 140.1, 135.7, 133.0, 132.8, 132.4, 131.4, 131.0, 130.7, 129.8, 129.2, 128.9, 128.8, 128.1, 127.4, 127.1, 123.0, 110.0, 42.1, 31.6, 29.4, 29.1, 29.0, 26.7, 22.6, 14.0; MALDI/TOF MS calcd for  $\text{C}_{64}\text{H}_{60}\text{N}_2\text{O}_4$  920.5, found 921.5. Anal. Calc. for  $\text{C}_{64}\text{H}_{60}\text{N}_2\text{O}_4$ : C, 83.45; H, 6.57; N, 3.04; Found: C, 83.40; H, 6.60; N, 3.03.

#### 2.2.6. 2,5-Dibutyl-3,6-bis(4'-((10-oxoanthracen-9(10H)-ylidene)methyl)phenyl)pyrrolo[3,4-c]pyrrole-1,4-dione (**4b**)

It was prepared by using the same synthetic procedure of **4a** to afford a red solid (**4b**) in 37% yield, m.p. 246–247 °C. FT-IR (KBr,

$\text{cm}^{-1}$ ): 3063, 3030, 2954, 2930, 2869, 1661, 1591, 1500, 1460, 1364, 1081, 835, 778, 734.  $^1\text{H}$  NMR (400 MHz,  $\text{CDCl}_3$ , ppm)  $\delta$  8.29–8.25 (m, 4H, Ar), 8.03 (d,  $J = 8.0$  Hz, 2H, Ar), 7.80 (d,  $J = 8.4$  Hz, 4H, Ar), 7.67 (t,  $J = 8.0$  Hz, 2H, Ar), 7.58–7.26 (m, 12H, Ar and C=CH), 7.25 (d,  $J = 6.0$  Hz, 2H, Ar), 3.78 (t,  $J = 7.6$  Hz, 4H,  $\text{NCH}_2$ ), 1.61–1.58 (m, 4H,  $\text{CH}_2$ ), 1.30–1.25 (m, 4H,  $\text{CH}_2$ ), 0.85 (t,  $J = 7.2$  Hz, 6H,  $\text{CH}_3$ );  $^{13}\text{C}$  NMR (100 MHz,  $\text{CDCl}_3$ , ppm)  $\delta$  184.6, 162.7, 147.8, 140.4, 140.2, 135.8, 133.1, 132.9, 132.5, 131.4, 131.0, 130.8, 129.8, 129.2, 129.0, 128.8, 128.2, 127.5, 127.2, 127.2, 123.1, 110.1, 41.8, 31.5, 20.0, 13.6; MALDI/TOF MS calcd for  $\text{C}_{56}\text{H}_{44}\text{N}_2\text{O}_4$  808.3, found 808.3. Anal. Calc. for  $\text{C}_{56}\text{H}_{44}\text{N}_2\text{O}_4$ : C, 83.14; H, 5.48; N, 3.46. Found: C, 83.23; H, 5.50; N, 3.47.

#### 2.2.7. 2,5-Dibenzyl-3,6-bis(4-((10-oxoanthracen-9(10H)-ylidene)methyl)phenyl)pyrrolo[3,4-c]pyrrole-1,4-dione(4c)

It was prepared by using the same synthetic procedure of **4a** to afford a red solid (**4c**) in 75.2% yield, m.p. 297–298 °C. FT-IR (KBr,  $\text{cm}^{-1}$ ): 3059, 3021, 1662, 1660, 1505, 1079, 773.  $^1\text{H}$  NMR (400 MHz,  $\text{CDCl}_3$ , ppm)  $\delta$  8.28–8.23 (m, 4H, Ar), 7.98 (d,  $J = 8.0$  Hz, 2H, Ar), 7.73 (d,  $J = 8.0$  Hz, 4H, Ar), 7.64 (t,  $J = 8.0$  Hz, 2H, Ar), 7.53–.37 (m, 12H, Ar and C=CH), 7.30–7.24 (m, 8H, Ar), 7.18 (d,  $J = 7.2$  Hz, 4H, Ar), 5.02 (s, 4H,  $\text{NCH}_2$ );  $^{13}\text{C}$  NMR (100 MHz,  $\text{CDCl}_3$ , ppm)  $\delta$  184.6, 162.7, 148.3, 140.6, 140.2, 137.3, 135.7, 133.1, 132.8, 132.4, 131.4, 131.0, 130.7, 129.8, 129.3, 129.2, 128.8, 128.2, 127.5, 127.2, 126.7, 123.1, 110.0, 45.7; MALDI/TOF MS calcd for  $\text{C}_{62}\text{H}_{40}\text{N}_2\text{O}_4$  876.3, found 876.3. Anal. Calc. for  $\text{C}_{62}\text{H}_{40}\text{N}_2\text{O}_4$ : C, 84.91; H, 4.60; N, 3.19. Found: C, 85.28; H, 4.60; N, 3.21.

#### 2.2.8. 2,5-Dioctyl-3,6-bis(4'-[2-(4-bromophenyl)-2-cyanovinyl]phenyl)pyrrolo[3,4-c] pyrrole-1,4-dione (5)

A mixture of 2-(4-bromophenyl)acetonitrile (122 mg, 0.625 mmol), **3a** (142 mg, 0.25 mmol), potassium carbonate (863 mg, 6.25 mmol) and absolute ethanol (4 mL) was heated under reflux for 2.5 h. After cooling, the mixture was poured into  $\text{H}_2\text{O}$  (5 mL). Precipitates were washed with water and recrystallized with  $\text{CH}_2\text{Cl}_2$  and methanol to afford a red solid (**5**) in 43% yield (100 mg), m.p. 263–264 °C. FT-IR (KBr,  $\text{cm}^{-1}$ ): 3064, 3030, 2952, 2921, 2853, 2220, 1677, 1589, 1505, 1464, 1379, 1096, 828, 726.  $^1\text{H}$  NMR (400 MHz,  $\text{CDCl}_3$ , ppm)  $\delta$  7.96 (d,  $J = 8.0$  Hz, 4H, Ar), 7.87 (d,  $J = 8.0$  Hz, 4H, Ar), 7.52–7.47 (m, 10H, Ar and C=CH), 3.76 (t,  $J = 7.2$  Hz, 4H,  $\text{NCH}_2$ ), 1.52 (m, 4H,  $\text{CH}_2$ ), 1.17 (m, 20H,  $\text{CH}_2$ ), 0.81 (t,  $J = 6.8$  Hz, 6H,  $\text{CH}_3$ );  $^{13}\text{C}$  NMR (100 MHz,  $\text{CDCl}_3$ , ppm)  $\delta$  162.4, 147.5, 140.6, 135.5, 132.8, 132.3, 129.8, 129.7, 129.4, 127.4, 124.0, 117.3, 111.8, 110.6, 41.9, 31.7, 29.4, 29.1, 29.0, 26.7, 22.6, 14.1; MS (APCI) calcd for  $\text{C}_{52}\text{H}_{52}\text{N}_4\text{O}_2\text{Br}_2$  924.2, found 925.7. Anal. Calc. for  $\text{C}_{52}\text{H}_{52}\text{N}_4\text{O}_2\text{Br}_2$ : C, 67.52; H, 5.67; N, 6.06. Found: C, 67.59; H, 5.70; N, 6.04.

### 2.3. Preparation of aggregates

Stock solutions of the DPP derivatives in THF with a concentration of 1 mM were prepared. Aliquots (100  $\mu\text{L}$ ) of the solution were transferred to volumetric flasks (10 mL). After adding appropriate amounts of THF, water was added dropwise at a constant rate of 1 mL/min under vigorous stirring to furnish 10  $\mu\text{M}$  solution with defined fractions of water ( $f_{\text{water}} = 0\text{--}90$  vol%). Spectral measurements of the resultant solutions or aggregate suspensions were performed immediately.

## 3. Result and discussion

### 3.1. Synthesis and structural characterization

The synthetic route employed to access the DPP derivatives is presented in Scheme 1. The key products **4** were obtained by a straightforward aldol-type condensation reaction of 9(10H)-anthracenone with appropriately formyl substituted DPP precursors in the presence of dry HCl/ethanol. However, attempts to

obtain **4** by using a condensation reaction in the presence of pyridine/piperidine failed [33]. Luminophores **2–4** are soluble in chloroform and tetrahydrofuran (THF), but insoluble in water.

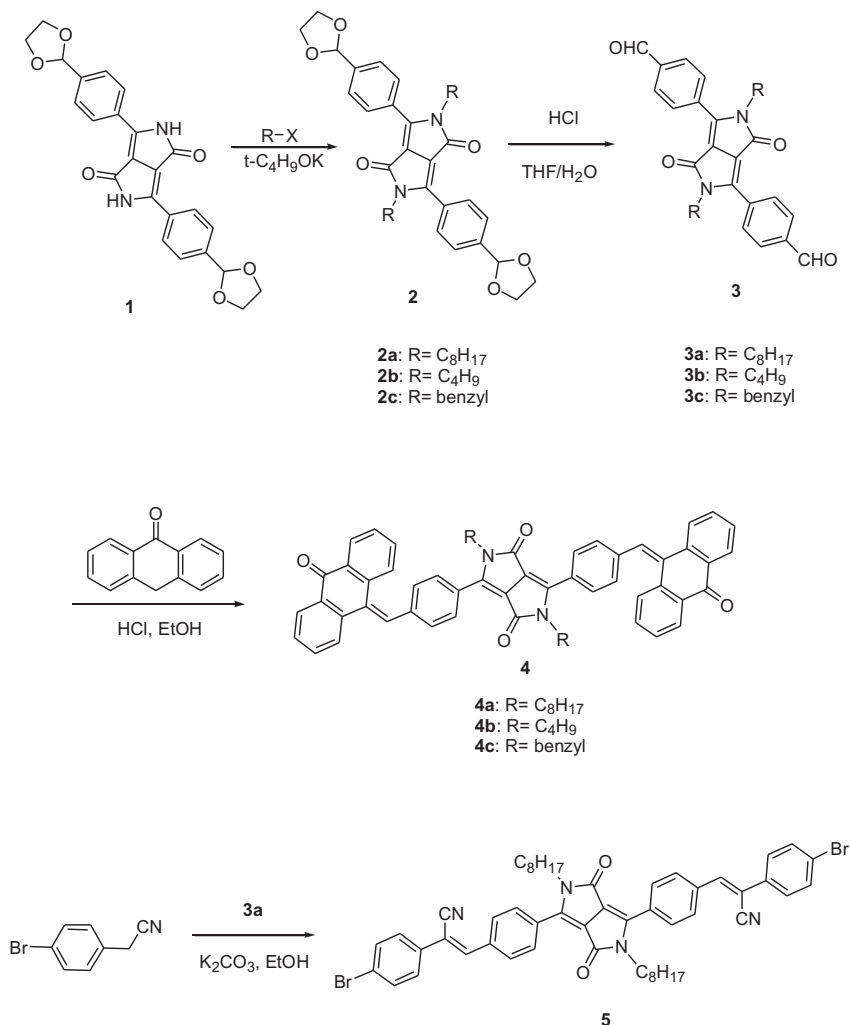
### 3.2. Photophysical properties

Compounds **2–5** had absorption peaks ( $\lambda_{\text{ab}}$ ) between 474 and 519 nm arising from the  $\pi\text{--}\pi^*$  transition of the DPP-ring moieties (Table 1). When changing substituents at the benzene ring with [1,3]dioxolanyl, aldehyde and anthracenone groups, respectively, the  $\lambda_{\text{ab}}$  of the DPP derivatives **2–4** was progressively red shifted due to their extended conjugated structures.

The solutions of **2a**, **3a** and **4a** had fluorescence maxima at 533, 570 and 597 nm with the efficiencies of 88%, 31% and 0.09% (Table 1), respectively. A similar trend was also observed in the series of **2b**, **3b**, **4b** and **2c**, **3c**, **4c** (Table 1). That is to say, the emission maximum ( $\lambda_{\text{em}}$ ) values of DPP derivatives were bathochromically shifted and their fluorescence quantum yields decreased, when changing substituents at the benzene ring from [1,3]dioxolanyl to aldehyde and anthracenone groups, respectively. The red-shifted  $\lambda_{\text{em}}$  should be attributed to the extended conjugated  $\pi$  systems. The decrease of efficiency might be due to the carbonyl groups which could increase the probability of inter-system crossing [34] and intramolecular rotation processes inducing annihilation of excitations [9,35]. However, the  $\lambda_{\text{em}}$  of the DPP molecules was blue-shifted and the fluorescence efficiency was enhanced when the 2,5-substituents were changed from octyl to butyl and benzyl. For example,  $\lambda_{\text{em}}$  of compounds **4a–c** was 654, 651 and 640 nm, respectively;  $\phi_{\text{F}}$  of **4a–c** was 0.09%, 0.17% and 0.36%, respectively. The reason for this phenomenon might be RIR [35]. The intramolecular rotation consumes energy and serves as a relaxation channel for the excited state to decay, which decrease the radiative decay [9]. Moreover, the ability of rotation and vibrational motion of the substituents on **2–4** decrease following the sequence of octyl, butyl and benzyl. Therefore, the fluorescence efficiency increases following this order.

A temperature dependence study of the emission properties of **4a** was conducted in THF solution. When a solution of **4a** was cooled from 20 to  $-70$  °C, its emission peak was slightly red shifted, and its emission intensity increased (Fig. 1). These experiments may confirm that the RIR process was a cause for the phenomenon observed in compounds **4a–c** since reducing the temperature would inhibit intramolecular rotation [9].

Comparison of the emission spectra of compounds in solution and in the solid state showed that crystals of all DPP derivatives exhibited bathochromic shifts. The extent of the spectral shift varied with molecular structure. Compounds **2c–4c** with benzyl substituents showed relatively small red shifts while **2b–4b** with a butyl substituent exhibited relatively larger shifts. This suggests that the bulky 2,5-substituents could reduce intermolecular interactions [8]. However, the fluorescence quantum yields of DPP derivatives in the solid state were different from those in solution. The fluorescence quantum yield ( $\phi_{\text{F}}$ ) of **2a**, **2b** and **2c** in crystals was 39%, 19% and 8.5%, respectively, which were much lower than that in solution. Their efficiencies decreased following the sequence of **2a**, **2b** and **2c**, which was contrary to the sequence in solution. Compounds **4a–c** were AIEE active because their PL intensities in the solid state were higher than those in solutions. Their emission intensities in the solid state were strongly affected by particle size and degree of crystallization. Therefore, their fluorescence quantum yields in crystals were not measured. The emission spectrum of **3a** in the solid state could not be obtained on the FL spectrophotometer. The crystals of **3b–c** and **5** emitted weakly. Their fluorescence quantum yields were not reported, considering the likely measurement error due to the measurement technique.



Scheme 1. Syntheses of DPP derivatives 2–5.

### 3.3. Aggregate-induced emission enhancement

Fluorescence properties of **4** were studied in various mixtures of THF and water (10  $\mu$ M) because compounds **4** were soluble in THF and insoluble in water (Fig. 2). The absorption spectra profiles of **4**

in the H<sub>2</sub>O/THF mixtures ( $f_{\text{water}} \geq 60\%$ ) showed a red-shift and a long absorption tail, which were characteristic of the nanoparticles' absorption [36]. Since the light-scattering effect of the aggregates of **4** in the aqueous mixtures made the quantum yield

**Table 1**  
Absorption and emission characteristics of DPP derivatives 2–5 in solutions and crystalline states.<sup>a</sup>

DPP derivatives	$\lambda_{\text{ab}}$ (nm)	$\epsilon$ (M <sup>-1</sup> cm <sup>-1</sup> )	$\lambda_{\text{em}}$ (nm)		$\phi_{\text{F}}$ (%)	
	Solution		Solution	Crystal	Solution <sup>b</sup>	Crystal <sup>c</sup>
<b>2a</b>	474	17,900	533	568	88 ± 2	39 ± 2
<b>3a</b>	498	11,300	570	570	31 ± 1	
<b>4a</b>	509	35,900	597	654	0.09 ± 0.01	
<b>2b</b>	474	16,863	533	570	97 ± 2	19 ± 2
<b>3b</b>	498	18,300	570	610	37 ± 1	
<b>4b</b>	507	33,700	597	651	0.17 ± 0.01	
<b>2c</b>	473	23,600	529	562	99 ± 2	8.5 ± 2
<b>3c</b>	496	21,500	565	604	45 ± 1	
<b>4c</b>	507	51,900	580	640	0.36 ± 0.01	
<b>5</b>	519	37,200	604	682	8.9 ± 0.3	

<sup>a</sup> Solution = 10  $\mu$ M in CHCl<sub>3</sub>,  $\lambda_{\text{ab}}$  = absorption maximum,  $\lambda_{\text{em}}$  = emission maximum,  $\phi_{\text{F}}$  = fluorescence quantum yield.

<sup>b</sup> Estimated using Rhodamine 6G ( $\phi_{\text{F}}$  = 95% in ethanol) as the standard,  $\lambda_{\text{ex}}$  = 488 nm.

<sup>c</sup> Measured using an integrating sphere.

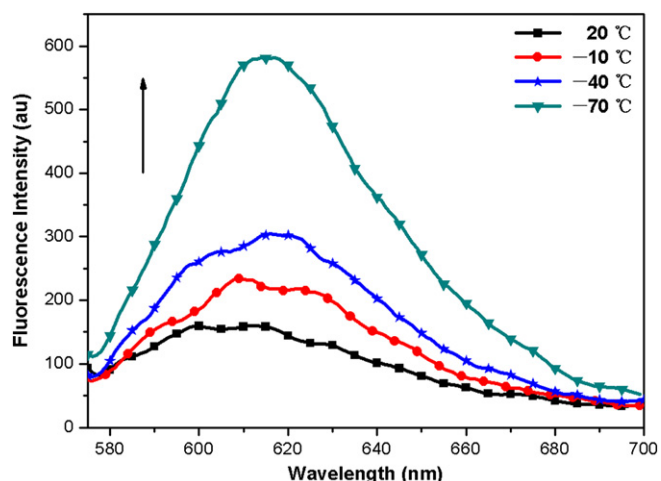
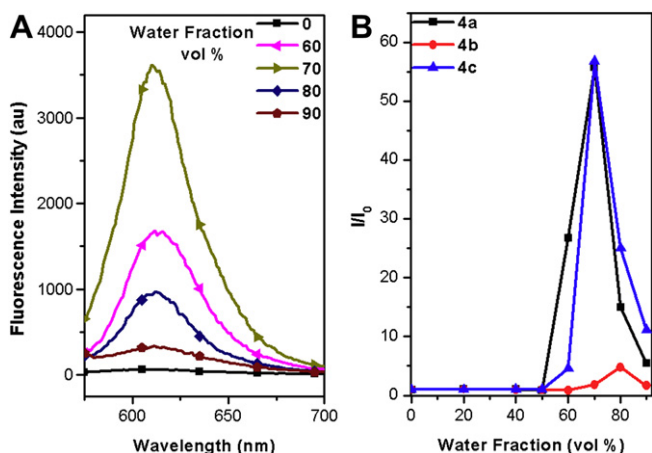


Fig. 1. Effect of temperature on emission of **4a** in THF solution (10  $\mu$ M,  $\lambda_{\text{ex}}$  = 560 nm).



**Fig. 2.** (A) Emission spectra of **4a** in H<sub>2</sub>O/THF mixtures. (B) Relations between the ratio of  $I/I_0$  and water fraction in H<sub>2</sub>O/THF mixtures.  $I_0$  and  $I$  were fluorescence peak intensity of **4** in pure THF and in H<sub>2</sub>O/THF mixtures (10  $\mu$ M), respectively; excitation wavelength: 560 nm for **4a**, 520 nm for **4b**, 552 nm for **4c**.

measurements inaccurate [36], the peak intensities of PL spectra were used for the comparison of their emission properties. The PL intensity of **4a** remained almost constant in the H<sub>2</sub>O/THF mixtures with up to 50% ( $f_{\text{water}}$ ), however, it increased sharply as the water content increased further (Fig. 2B). The PL intensity of **4a** in the 70% ( $f_{\text{water}}$ ) H<sub>2</sub>O/THF mixture was about 55 times higher than that in THF solution. Moreover, **4a** would gradually aggregate in the H<sub>2</sub>O/THF mixtures with increase of water content. Therefore, **4a** is AIEE active [9].  $\lambda_{\text{em}}$  and full width at half maximum of PL of **4a** were similar in H<sub>2</sub>O/THF at different water content. Similar trends were observed for **4b** and **4c**. However, the increments of PL intensity depended on the 2,5-substituents of the DPP-ring (Fig. 2). As shown in Fig. 2B, the maximum of  $I/I_0$  of **4a–c** was 56, 4.8 and 57, respectively.

The emission intensity of **4** decreased as the fraction of water further increased in the H<sub>2</sub>O/THF mixtures. For example, the ratio of  $I/I_0$  of **4a** decreased from 56 to 5 as the water fraction increased from 70% to 90%. This could be attributed to a morphology change in the aggregates of **4** in the aqueous medium [10]. During the process of preparation of aggregates, water was added at a constant rate to the THF solutions of **4**. As a result, in the H<sub>2</sub>O/THF mixtures of low water content (e.g.,  $f_{\text{water}} \leq 70\%$ ), the molecules of luminophores may aggregate slowly, which could form more crystalline particles and less amorphous aggregates. However, in the mixtures with high water content (e.g.,  $f_{\text{water}} > 80\%$ ), the molecules of luminophores might aggregate abruptly, which might form more amorphous aggregates and lead to a low ratio of crystalline particles [10]. The quantum yield of the crystalline particles might be higher than that of the amorphous particles [10]. Therefore, PL intensity of **4** would decrease with a higher fraction of water.

In order to confirm this hypothesis, an amorphous thin film of **4a** was prepared by melting a sample of **4a** on a quartz plate under N<sub>2</sub>. Since solvent fuming can induce chromophores to crystallize [10], the emission intensity transformation of **4a** with different crystallization degree could be tracked by fuming the amorphous thin film with organic solvent vapor. As shown in Fig. 3, the fluorescence intensity of the thin film of **4a** was significantly enhanced by fuming with CH<sub>2</sub>Cl<sub>2</sub> vapor, while the intensity of **3a** was almost unchanged. The morphological structures of the parent and fumed films were checked by polarized light microscope (POM), confirming the hypothesis that fuming-induced crystallization was responsible for the emission enhancement. The untreated film showed a uniform dark shade under POM observation, while the

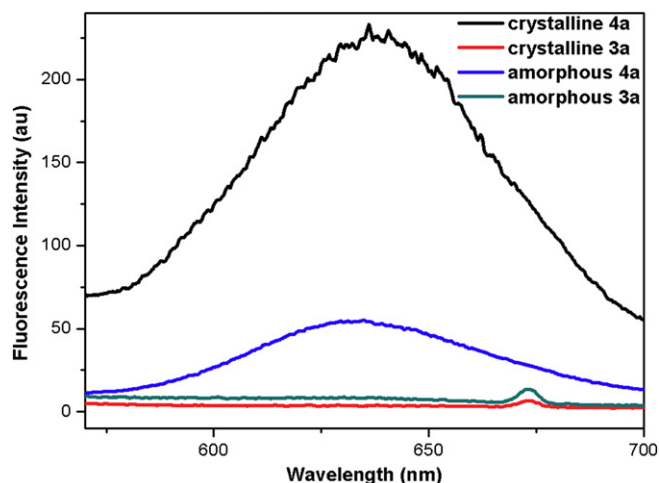


**Fig. 3.** Emission spectra of amorphous and crystalline films of luminophore **3a** ( $\lambda_{\text{ex}} = 450$  nm) and **4a** ( $\lambda_{\text{ex}} = 560$  nm).

treated film displayed birefringent textures. Based on these observations, **4a** was considered to be CIEE active. Furthermore, vapor-responsiveness of the PL of **4a** could enable it to find application in detecting volatile organic compounds (VOCs) [10].

The fluorescence properties of **4c** were compared with those of **2c**, **3c** and **5** that contained different substituents at the 3- and the 6-positions of the DPP unit (Fig. 2B vs Fig. 4). It was found that only **4c** possessing anthracenone groups was AIEE active.

#### 3.4. Crystal structures and mechanism

Single crystals of **3c** and **4c** were grown from CH<sub>2</sub>Cl<sub>2</sub>/EtOAc and CH<sub>2</sub>Cl<sub>2</sub>/*n*-hexane, respectively, and were analyzed by X-ray diffraction crystallography. Their crystal structures are shown in Fig. 5, and detailed crystal data are given (see Supporting Information in Table S1).

In the crystal structure of **4c** (Fig. 5), anthracenone groups are strongly distorted (the dihedral angle between two phenyls of the anthracenone group is 26.4°) due to the steric hindrance between H1 and H2 ( $d = 2.036$  Å). The dihedral angle between the anthracenone

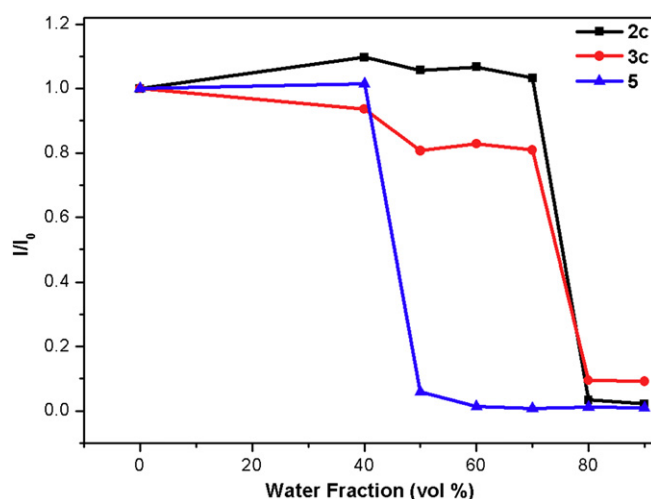


**Fig. 4.** Relations between the ratio of  $I/I_0$  and water fraction in H<sub>2</sub>O/THF mixtures.  $I_0$  and  $I$  were fluorescence peak intensity of **2c**, **3c** and **5** in pure THF and in H<sub>2</sub>O/THF mixtures (10  $\mu$ M), respectively; excitation wavelength: 485 nm for **2c**, 510 nm for **3c**, 540 nm for **5**.

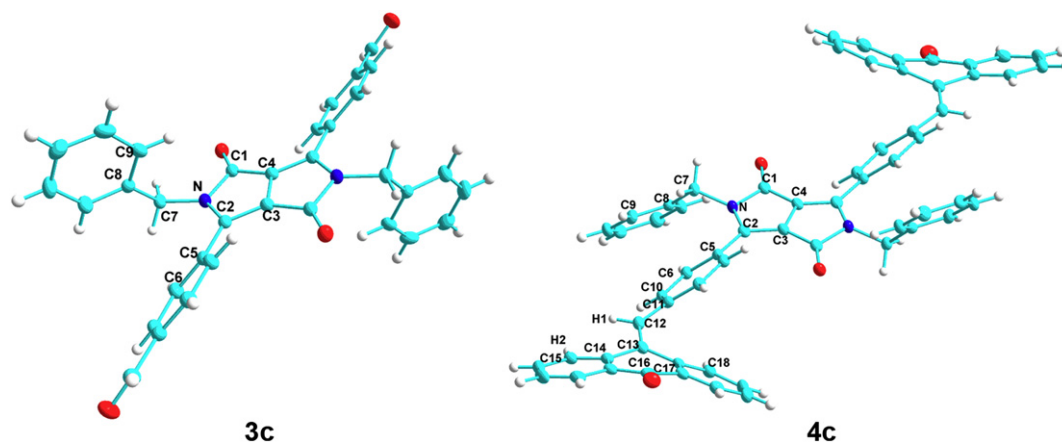


Fig. 5. Single crystal structures of **3c** and **4c**.

groups and the middle benzene ring is  $41.6^\circ$ . The dihedral angle ( $\theta = 39.7^\circ$ ) between the DPP-ring and the benzene ring is nearly equal to that of **3c** ( $\theta = 40.2^\circ$ ). The angle between N–C7 bond and the DPP-ring is  $72.1^\circ$ , while the angle between the C8–C7 bond and the DPP-ring is  $135.4^\circ$ . These angles are larger than the corresponding ones of **3c** ( $28.0^\circ$  and  $100.5^\circ$ , respectively), that could be attributed to the effect of the anthracenone groups.

As shown in Fig. 6a, the molecules of **3c** pack into “zigzag motif” in one layer. The stacking arrangement of **3c** is shown in Fig. 6b. The distance between the C=O double bond of aldehyde group and the DPP-ring of neighboring molecule is  $3.836 \text{ \AA}$ , and the distance of two phenyl rings is  $3.852 \text{ \AA}$ , indicating that the dimer has weak  $\pi$ – $\pi$  interactions. In addition, two aromatic C–H $\cdots$ O hydrogen bonds with distances of  $2.443 \text{ \AA}$  are observed in the dimer.

The arrangement of **4c** in the crystal is significantly different from that of **3c** as shown in Fig. 7. Two layers of **4c** are arranged in a “V” shaped fashion while layers of **3c** adopt a nearly linear arrangement. The distance between the C=O double bond of anthracenone groups and the DPP-ring of neighboring molecule is  $3.426 \text{ \AA}$  (Fig. 7c), while the distance of two anthracenone groups is  $3.723 \text{ \AA}$  (Fig. 7d). These  $\pi$ – $\pi$  interaction distances are shorter than those in **3c**. Therefore, the molecules of **4c** should have stronger  $\pi$ – $\pi$  interactions than those of **3c**. This could be used to explain the phenomenon that the angle between N–C7 bond and the DPP-ring, and the angle between the C8–C7 bond and the DPP-ring of **4c** are larger than the corresponding angles of **3c**. Moreover four CH– $\pi$  interactions with interaction distances of  $3.166$ ,  $3.166$ ,  $2.943$  and  $2.943 \text{ \AA}$  exist in the dimers of **4c** (Fig. 7c and d), but such

interactions were not found in the dimer of **3c**. These CH– $\pi$  interactions may lead to relatively tight packing and rigid molecules of **4c** in the crystals [37].

Generally,  $\pi$ – $\pi$  aggregation in the solid state could quench the emission of organic luminophores due to the formation of detrimental excimers [5,7,8,38]. That is to say, the degree of fluorescence quenching would increase with the stronger  $\pi$ – $\pi$  stacking of the luminogenic molecules. As discussed above, it is clear that stronger  $\pi$ – $\pi$  interactions exist among the molecules of **4c** than among those of **3c** in crystals. From this point of view, compound **4c** should have a stronger fluorescence quenching behavior than **3c** from the solution to the solid state. However, the experimental results showed that **4c** exhibited significant enhancement of its light-emission from the solution to the solid state while the emission intensity of **3c** decreased. What should be responsible for this phenomenon? Besides  $\pi$ – $\pi$  interactions, other interactions also exist among the molecules of **3c** and **4c** in crystals such as hydrogen bond interactions and CH– $\pi$  interactions, which would inhibit intramolecular rotation. Although two aromatic C–H $\cdots$ O hydrogen bond interactions exist in the dimer of **3c**, they are too weak to hold the molecules of **3c** tightly in crystal lattice [39]. In other words, intramolecular rotation might still cause the non-radiative decay of excited state of **3c** in the solid state [9]. In contrast, many CH– $\pi$  interactions exist among the molecules of **4c** in crystals, which could block intramolecular rotation and enhance the radiative decay [9]. The restriction of intramolecular rotation (RIR) could increase emission intensity while  $\pi$ – $\pi$  aggregation could induce fluorescence quenching. The results of the competition between

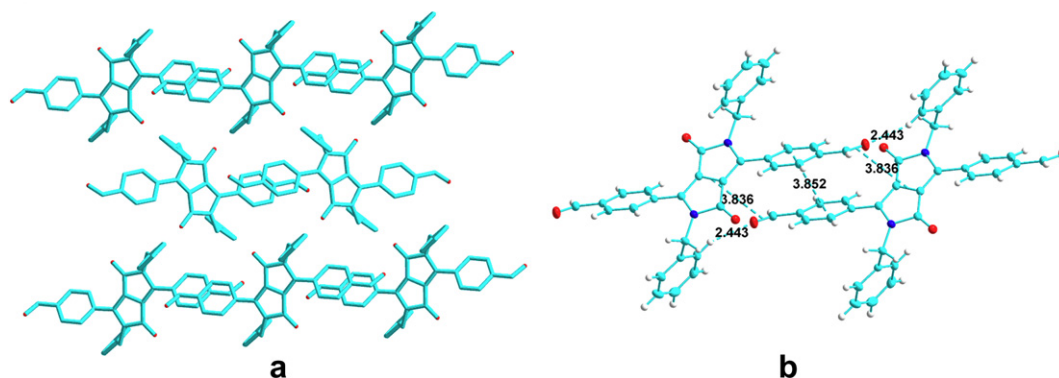
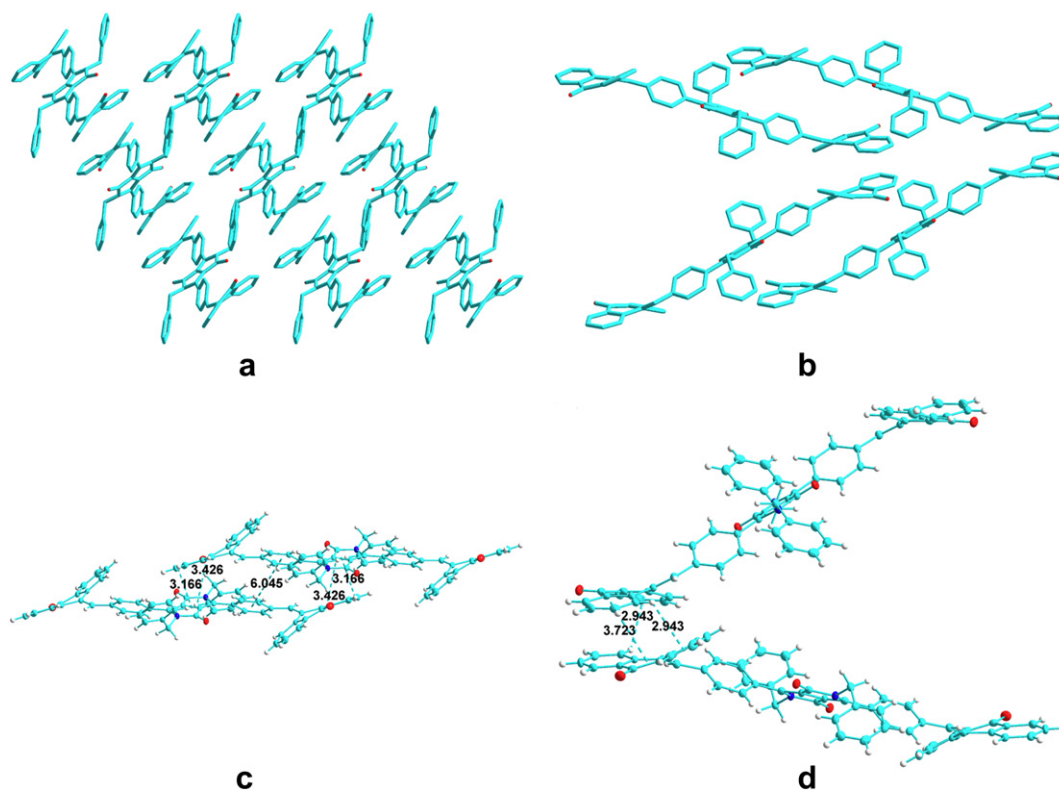


Fig. 6. (a) Stacking images of **3c**, a-axis view. The hydrogen atoms have been omitted for clarity. (b) The intermolecular interactions of **3c** in the crystals.



**Fig. 7.** (a) Stacking images of **4c**, b-axis view. (b) A tetramer unit of **4c**, a<sup>+</sup>-axis view. The hydrogen atoms have been omitted for clarity. (c–d) The intermolecular interactions of **4c** in the crystals.

the RIR and  $\pi$ – $\pi$  aggregation were different for **3c** and **4c**. The fluorescence intensity of **3c** was remarkably decreased with the increased accumulation of its molecules, while the emission intensity of **4c** was augmented with the formation of molecular aggregation. Moreover, the degree of the conformational stiffening caused by the restricted intramolecular rotation in the crystalline state of **4c** was higher than that in amorphous particles. Therefore **4c** exhibited CIEE [10].

As for **4b**,  $\pi$ – $\pi$  aggregation between anthracenone groups and the emission group (DPP-ring) should be stronger than that of **4a** and **4c**, due to the weak steric hindrance of butyl group. Therefore, its AIEE effect is weak.

The analysis of the crystal structures of **3c** and **4c** demonstrates that supramolecular interactions affect the degree of torsion and stacking feature of the molecules. The variation of the  $\pi$ -conjugated units and steric hindrance of substituents linked to the DPP-ring could affect the packing model and photophysical properties in the solid states.

#### 4. Conclusion

A series of DPP derivatives were synthesized and their fluorescence properties in solution and solid state were investigated. PL spectra and quantum yields of the chromophores were found to be tunable by changing the  $\pi$ -conjugated units and alkyl groups linked to the DPP-ring. In solution, the extended conjugated  $\pi$  system could make a bathochromic shift in the emission spectrum, meanwhile, the PL efficiency of the chromophore would decrease due to carbonyl groups and intramolecular rotation processes inducing annihilation of excitations; the quantum yields of the luminescent moieties would decrease with the increased rotation motion of alkyl substituents. However, the fluorescence quantum yields of DPP derivatives in the crystals were different from those in

solution. The fluorescence intensities of **2a–2c**, **3a–3c** and **5** decreased while fluorescence intensities of **4a–4c** increased. The quantum yields of luminescent molecules in the solid state were controlled by the competition between RIR causing emission enhancement and  $\pi$ – $\pi$  aggregation inducing fluorescence quenching. The conformational stiffening caused by the restricted intramolecular rotation in the crystals of **4** was higher than that in the amorphous particles, which depicted that **4** possessed CIEE. These results are important in molecular design to gain expected fluorescence properties in solution and solid state. Furthermore, vapor-responsiveness of the PL of **4** could enable it to find application in detecting VOCs.

#### Acknowledgment

This work was supported by the National Natural Science Foundation of China (20872038, 20904010), the Fundamental Research Funds for the Central Universities (2009ZM0170) and the Natural Science Foundation of Guangdong Province, China (10351064101000000).

#### Appendix. Supporting information

Supplementary data related to this article can be found online at doi:10.1016/j.dyepig.2011.01.005.

#### References

- [1] Bouffard J, Kim Y, Swager TM, Weissleder R, Hilderbrand SA. A highly selective fluorescent probe for thiol bioimaging. *Org Lett* 2008;10:37–40.
- [2] Picot A, D'Aleo A, Baldeck PL, Grichine A, Duperray A, Andraud C, et al. Long-lived two-photon excited luminescence of water-soluble europium complex: applications in biological imaging using two-photon scanning microscopy. *J Am Chem Soc* 2008;130:1532–3.

- [3] Liu Y, Tao X, Wang F, Dang X, Zou D, Ren Y, et al. Aggregation-induced emissions of fluorenonearylamine derivatives: a new kind of materials for non-doped red organic light-emitting diodes. *J Phys Chem C* 2008;112:3975–81.
- [4] Grimsdale AC, Leok Chan K, Martin RE, Jokisz PG, Holmes AB. Synthesis of light-emitting conjugated polymers for applications in electroluminescent devices. *Chem Rev* 2009;109:897–1091.
- [5] An BK, Kwon SK, Jung SD, Park SY. Enhanced emission and its switching in fluorescent organic nanoparticles. *J Am Chem Soc* 2002;124:14410–5.
- [6] Crenshaw BR, Weder C. Deformation-induced color changes in melt-processed photoluminescent polymer blends. *Chem Mater* 2003;15:4717–24.
- [7] Yuan CX, Tao XT, Ren Y, Li Y, Yang JX, Yu WT, et al. Synthesis, structure, and aggregation-induced emission of a novel lambda (Lambda)-shaped pyridinium salt based on Troger's base. *J Phys Chem C* 2007;111:12811–6.
- [8] Zhao ZJ, Wang ZM, Lu P, Chan CYK, Liu DD, Lam JWY, et al. Structural modulation of solid-state emission of 2,5-bis(trialkylsilylethynyl)-3,4-diphenylsiloles. *Angew Chem Int Ed* 2009;48:7608–11.
- [9] Hong YN, Lam JWY, Tang BZ. Aggregation-induced emission: phenomenon, mechanism and applications. *Chem Commun*; 2009:4332–53.
- [10] Qian LJ, Tong B, Shen JB, Shi JB, Zhi JG, Dong YQ, et al. Crystallization-induced emission enhancement in a phosphorus-containing heterocyclic luminogen. *J Phys Chem B* 2009;113:9098–103.
- [11] Wang Z, Shao H, Ye J, Tang L, Lu P. Dibenzosuberonylidene-ended fluorophores: rapid and efficient synthesis, characterization, and aggregation-induced emissions. *J Phys Chem B* 2005;109:19627–33.
- [12] Tang WX, Xiang Y, Tong AJ. Salicylaldehyde azines as fluorophores of aggregation-induced emission enhancement characteristics. *J Org Chem* 2009;74:2163–6.
- [13] Zhou TL, Li F, Fan Y, Song WF, Mu XY, Zhang HY, et al. Hydrogen-bonded dimer stacking induced emission of aminobenzoic acid compounds. *Chem Commun*; 2009:3199–201.
- [14] Xie Z, Yang B, Xie W, Liu L, Shen F, Wang H, et al. A class of nonplanar conjugated compounds with aggregation-induced emission: structural and optical properties of 2,5-diphenyl-1,4-distyrylbenzene derivatives with all cis double bonds. *J Phys Chem B* 2006;110:20993–1000.
- [15] Zeng Q, Li Z, Dong YQ, Di CA, Qin AJ, Hong YN, et al. Fluorescence enhancements of benzene-cored luminophors by restricted intramolecular rotations: AIE and AIEE effects. *Chem Commun*; 2007:70–2.
- [16] Yuan WZ, Zhao H, Shen XY, Mahtab F, Lam JWY, Sun JZ, et al. Luminogenic polyacetylenes and conjugated polyelectrolytes: synthesis, hybridization with carbon nanotubes, aggregation-induced emission, superamplification in emission quenching by explosives, and fluorescent assay for protein quantitation. *Macromolecules* 2009;42:9400–11.
- [17] Yao H, Yamashita M, Kimura K. Organic styryl dye nanoparticles: synthesis and unique spectroscopic properties. *Langmuir* 2009;25:1131–7.
- [18] Hu R, Lager E, Aguilar-Aguilar AL, Liu J, Lam JWY, Sung HHY, et al. Twisted intramolecular charge transfer and aggregation-induced emission of BODIPY derivatives. *J Phys Chem C* 2009;113:15845–53.
- [19] Ren Y, Dong Y, Lam JWY, Tang BZ, Wong KS. Studies on the aggregation-induced emission of silole film and crystal by time-resolved fluorescence technique. *Chem Phys Lett* 2005;402:468–73.
- [20] Ren Y, Lam JWY, Dong Y, Tang BZ, Wong KS. Enhanced emission efficiency and excited state lifetime due to restricted intramolecular motion in silole aggregates. *J Phys Chem B* 2005;109:1135–40.
- [21] Peng Q, Yi YP, Shuai ZG, Shao JS. Toward quantitative prediction of molecular fluorescence quantum efficiency: role of duschinsky rotation. *J Am Chem Soc* 2007;129:9333–9.
- [22] Xie Z, Xie W, Li F, Liu L, Wang H, Ma Y. Controlling supramolecular microstructure to realize highly efficient nondoped deep blue organic light-emitting devices: the role of diphenyl substituents in distyrylbenzene derivatives. *J Phys Chem C* 2008;112:9066–71.
- [23] Xie ZQ, Wang H, Li F, Xie WJ, Liu LL, Yang B, et al. Crystal structure of a highly luminescent slice crystal grown in the vapor phase: a new polymorph of 2,5-diphenyl-1,4-distyrylbenzene. *Cryst Growth Des* 2007;7:2512–6.
- [24] Gao B-R, Wang H-Y, Hao Y-W, Fu L-M, Fang H-H, Jiang Y, et al. Time-resolved fluorescence study of aggregation-induced emission enhancement by restriction of intramolecular charge transfer state. *J Phys Chem B* 2010;114:128–34.
- [25] Wang F, Han MY, Mya KY, Wang YB, Lai YH. Aggregation-driven growth of size-tunable organic nanoparticles using electronically altered conjugated polymers. *J Am Chem Soc* 2005;127:10350–5.
- [26] Kumar NSS, Varghese S, Suresh CH, Rath NP, Das S. Correlation between solid-state photophysical properties and molecular packing in a series of indane-1,3-dione containing butadiene derivatives. *J Phys Chem C* 2009;113:11927–35.
- [27] Davis R, Saleesh Kumar NS, Abraham S, Suresh CH, Rath NP, Tamaoki N, et al. Molecular packing and solid-state fluorescence of alkoxy-cyano substituted diphenylbutadienes: structure of the luminescent aggregates. *J Phys Chem C* 2008;112:2137–46.
- [28] Cao DR, Liu QL, Zeng WJ, Han SH, Peng JB, Liu SP. Diketopyrrolopyrrole-containing polyfluorenes: facile method to tune emission color and improve electron affinity. *Macromolecules* 2006;39:8347–55.
- [29] Jin Y, Xu Y, Qiao Z, Peng J, Wang B, Cao D. Enhancement of electroluminescence properties of red diketopyrrolopyrrole-doped copolymers by oxadiazole and carbazole units as pendants. *Polymer* 2010;51:5726–33.
- [30] Li B, Miao WR, Cheng LB. Synthesis and fluorescence properties of 9,10-bis(phenylethynyl)anthracenes. *Dyes Pigments* 1999;43:161–5.
- [31] Demas JN, Crosby GA. Measurement of photoluminescence quantum yields, a review. *J Phys Chem* 1971;75:991–1024.
- [32] Qiao Z, Xu YB, Lin SM, Peng JB, Cao DR. Synthesis and characterization of red-emitting diketopyrrolopyrrole-alt-phenylenevinylene polymers. *Synth Met* 2010;160:1544–50.
- [33] Prinz H, Ishii Y, Hirano T, Stoiber T, Camacho Gomez JA, Schmidt P, et al. Novel benzyliidene-9(10H)-anthracenones as highly active antimicrotubule agents. synthesis, antiproliferative activity, and inhibition of tubulin polymerization. *J Med Chem* 2003;46:3382–94.
- [34] Valeur B. *Molecular fluorescence: principles and applications*. New York: Wiley-VCH; 2001.
- [35] Dong S, Li Z, Qin J. New carbazole-based fluorophores: synthesis, characterization, and aggregation-induced emission enhancement. *J Phys Chem B* 2009;113:434–41.
- [36] Liu Y, Tao XT, Wang FZ, Shi JH, Sun JL, Yu WT, et al. Intermolecular hydrogen bonds induce highly emissive excimers: enhancement of solid-state luminescence. *J Phys Chem C* 2007;111:6544–9.
- [37] He JT, Xu B, Chen FP, Xia HJ, Li KP, Ye L, et al. Aggregation-induced emission in the crystals of 9,10-distyrylanthracene derivatives: the essential role of restricted intramolecular torsion. *J Phys Chem C* 2009;113:9892–9.
- [38] Ozdemir T, Atilgan S, Kutuk I, Yildirim LT, Tulek A, Bayindir M, et al. Solid-state emissive BODIPY dyes with bulky substituents as spacers. *Org Lett* 2009;11:2105–7.
- [39] Yuan WZ, Shen XY, Zhao H, Lam JWY, Tang L, Lu P, et al. Crystallization-induced phosphorescence of pure organic luminogens at room temperature. *J Phys Chem C* 2010;114:6090–9.